Electromagnetic Compatibility of Power Line Communications in Energy Storage Units

Gautham Prasad, Yinjia Huo, Lutz Lampe, and Victor C. M. Leung
The University of British Columbia, Vancouver, BC.
Email: {gauthamp, yortka}@ece.ubc.ca

***Abstract*—Increasing integration of renewable forms of energy production has prompted a significant growth in storage technologies to address the intermittent nature of renewable energy generation. Due to the ubiquitous nature of power cables in this environment, power line communications (PLC) is a natural solution to enable robust wired communication in energy management systems. In this paper, we address electromagnetic compatibility (EMC) issues for such systems. We begin by modeling the power cables as transmitting and receiving antennas to determine the impact of radiated emissions caused by PLC on neighboring applications. By illustrating the uniqueness associated with PLC applied in an energy storage unit, we use the standardized EMC limits to determine the maximum feeding signal strength that can be allowed on battery cables. Further, we characterize the electromagnetic interference caused by the PLC signal on nearby wired communication networks, and in particular, derive the interference power spectral density levels that are radiated onto neighboring broadband PLC communications.**

I. Introduction

The growth of distributed energy generation through renewable sources demands increased energy storage abilities due to the irregular and discontinuous nature of renewable energy generation [1]–[3]. On a smaller scale, battery storage facilities can also be found in road and rail transport applications [4], [5]. In all these use-cases, the battery storage units are equipped with a digital battery management system (BMS) that primarily achieves cell monitoring, cell balancing, ensuring battery safety and protection, state-of-health estimation, charging control, and thermal management [6, and references therein]. The BMS is therefore required to constantly monitor the voltage, temperature, and state-of-charge of all cells in the unit. This is typically achieved by using cell-boards that monitor these parameters of individual batteries and convey it to a central battery control unit (BCU). Conventional BMSs use dedicated cables to enable bidirectional communication between the cell-boards and the BCU [7]. Alternatively, the physical architecture can be simplified by using power line communications (PLC), which exploits the existing infrastructure, i.e., battery power cables, to provide robust and cost-efficient communications [8]–[10].

One of the fundamental aspects that has regulated PLC in any field of application from home area networks to smart-grid communications is its associated electromagnetic interference (EMI) and susceptibility [11]. Although recent works have demonstrated the feasibility of PLC for communications in BMSs in the context of both electric vehicles and grid storage facilities [12]–[14], the issues of electromagnetic compatibility (EMC) of PLC inside these energy storage units is not well-investigated. Apart from the need to comply with regulatory EMC limits, the issue of EMI is especially important in battery storage units at distributed generation locations, where multiple cell-boards that are part of different heterogeneous communication networks operate in close proximity. Furthermore, PLC radiations could also interfere with neighboring wired communication networks, such as broadband PLC operating in the smart-grid or indoor environment.

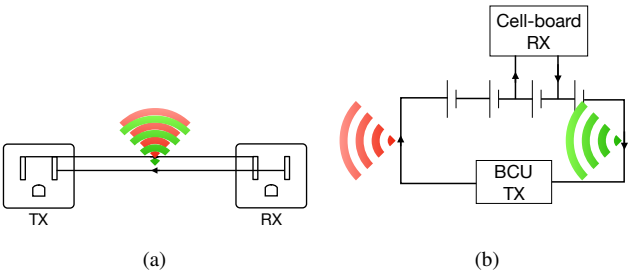

Fig. 1. Illustrations of (a) the fields generated by signals in opposing directions interfering destructively in conventional PLC, and (b) cables carrying signals in opposing directions being too far away from each other for their fields to completely cancel each other out in PLC-B.

Various facets of EMI in power line networks have already been extensively studied in the literature, e.g., [15]–[18]. However, we notice a crucial difference in the architectures of traditional PLC and PLC for BMSs (referred to as PLC-B hereafter), as illustrated in Fig. 1. For traditional PLC, where the conductors carrying the outgoing and return signals are bundled together, the radiation effects of the differential-mode (DM) signals cancel each other out. As a result, the common-mode (CM) signal is the primary source of electromagnetic radiation. On the other hand, in PLC-B scenarios, the feeding conductor and return conductor could be spaced wide apart from each other (e.g., Fig. 1(b); also see [13, Figs. 1 and 10]). This leads to negligible destructive interference of the electromagnetic (EM) radiations. Thus, a signal of the same strength causes much stronger net radiation in PLC-B vis-a-vis conventional PLC. Therefore, the transmission limits imposed

This work was supported by the Natural Sciences and Engineering Research Council of Canada (NSERC).

on conventional PLC transmission is not directly applicable to PLC-B systems.

Contributions: In this paper, we investigate the effects of EMI caused by PLC-B in an energy storage unit. We first use the transmission line theory with the method-of-images to model the signal propagation over the battery cable. Next, we represent the conductor as a concatenation of several infinitesimally small Hertzian dipoles to compute the radiated electric field at any point in space. We then use the electric field limits imposed by the U.S. Federal Communications Commission (FCC) regulations for radiated emissions [19], and determine the maximum permissible PLC signal strength that can be injected into the cable[1]. Further, we investigate the impact of the injected PLC-B signal on a neighboring broadband PLC network, by modeling the power line as a non-ideal receiving antenna. We use measured reception factor values reported in the literature to determine the interference signal magnitude that is radiated into a nearby broadband PLC application as a result of a PLC-B transmission. Finally, we suggest usable transmission signal strength limits that not only conform to the FCC standards, but also cause benign interference on neighboring broadband PLC networks.

II. EMI Formulation

We consider a battery storage unit where multiple cells are connected in both series and parallel to obtain the desired current and voltage levels. Every cell has a cell-board connected between the positive and negative terminals of the battery [8, Fig. 1.2]. The central BCU has the ability to communicate individually to each of these cell-boards in a master-slave topology to enable operations such as cell balancing and charging control [13] [8, Ch. 3]. As a result, the outgoing and return current paths are not physically close to each other. This leads to unintentional radiation that is not canceled by opposing fields.

A. Current Propagation Model

EM radiation is quantified by the magnitude of the radiated electric field, $\left|\vec{\boldsymbol{E}}(f)\right|$, at any given distance for a frequency[2] f. To compute $\vec{\boldsymbol{E}}$ radiated from a power cable, we consider a single conductor with current I flowing through it. However, in general, there could be multiple conductors in close proximity with each other that connect different cells with each other and the BCU. Since we are interested in determining the electric field strength at a distance that is significantly larger than the dimensions of the cable, we can view this as a single conductor with an effective radius of r_{eff} and a net cross-sectional current of I_{net} [21].

Further, as the cross-sectional dimensions of the cable are also electrically small compared to the wavelength of PLC signal, I_{net} can be viewed as propagating with the quasi-transverse-electromagnetic mode along the wire, which can be modeled using transmission line (TL) theory [22, Ch. 1]. The TL theory models the propagation of currents by TL equations using the per-unit-length (PUL) parameters of the cable. In the following, we derive the PUL parameters of resistance (R), inductance (L), capacitance (C) and conductance (G) for our considered scenario.

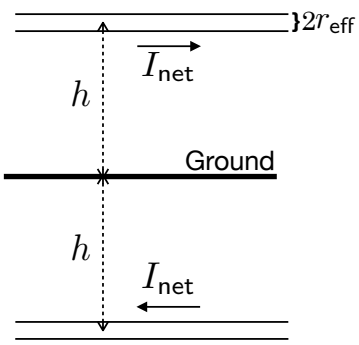

Fig. 2. The method-of-images model for a single conductor that is at a height h above the ground plane and carrying a current I_{net}.

For the current propagation similar to what is shown in Fig. 1(b), we can view the condition as a current flow in a single conductor over the ground plane with height h, which can be modeled by TL theory using the method of images [22, Ch. 4]. This setup is also shown in Fig. 2. Using the method of images, the considered scenario is equivalent to replacing the ground plane with an identical conductor that is symmetrical with respect to ground, i.e., an identical conductor is placed below the ground plane with a height h and the two conductors lie on the same vertical plane. In addition, the conductor below the ground plane has a current $-I_{\text{net}}$ flowing through. We also consider the conductor to be cylindrical, and the surrounding medium to be non-ferromagnetic so that the permeability of the surrounding medium equals that of free space, i.e. $\mu = \mu_0$.

The computation of R depends on the relationship between r_{eff} and the skin depth, δ, which is defined as

$$\delta = \frac{1}{\sqrt{f\pi\mu\sigma_{\text{cond}}}}, \tag{1}$$

where σ_{cond} is the conductance of the conductor. For a copper conductor, $\sigma_{\text{cond}} = 5.96 \times 10^7$ S, and thus, the maximum value of δ over the considered frequency range of 1.8 MHz to 30 MHz is $\delta_{\max} = 4.86 \times 10^{-5}$ m. Since $\delta_{\max} \ll r_{\text{eff}}$, we use [22, Eq. 4.103b] to calculate R as

$$R = \frac{1}{2r_{\text{eff}}\pi\sigma_{\text{cond}}\delta}. \tag{2}$$

Next, for the computation of L, C, and G, we consider $h \gg 2r_{\text{eff}}$, which is clearly a typically observable condition (see Fig. 2). For computational simplicity, we approximate the medium to be homogeneous in the insulation permittivity, ϵ_{ins}, and insulation conductance, σ_{ins}. Under such conditions, we

[1] Although we use the FCC regulations, the same procedure that we present can also be used to obtain transmission limits for any given specifications. We choose to apply the FCC regulation as it explicitly specifies the maximum permissible field strength levels for radiated emissions, while European regulations, such as EN 50561, indicate the value through conducted emissions [20].

[2] Henceforth, until we present numerical results in Section IV, we drop the indexing of f for brevity.

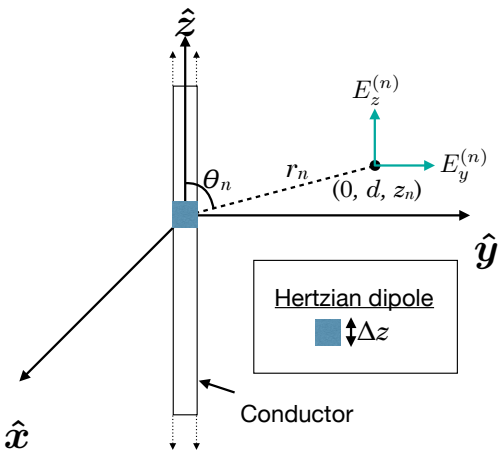

Fig. 3. The Cartesian coordinates representation of the electric field produced at a distance d from the conductor by its nth dipole element that is oriented along the z-axis.

obtain the closed form expressions for the PUL parameters as [22, Eq. 4.45 - 4.47]

$$C = \frac{2\pi\epsilon_{\mathsf{ins}}}{\ln\left(\frac{2h}{r_{\mathsf{eff}}}\right)}, \tag{3}$$

$$L = \frac{\mu}{2\pi}\ln\left(\frac{2h}{r_{\mathsf{eff}}}\right), \tag{4}$$

$$G = \frac{2\pi\sigma_{\mathsf{ins}}}{\ln\left(\frac{2h}{r_{\mathsf{eff}}}\right)}. \tag{5}$$

Typically, cable insulation materials are characterized with the complex relative permittivity, ϵ_{comp}. In such cases, we have $\epsilon_{\mathsf{ins}} = \epsilon_0\Re\{\epsilon_{\mathsf{comp}}\}$ and $\sigma_{\mathsf{ins}} = -2\pi f\epsilon_0\Im\{\epsilon_{\mathsf{comp}}\}$, where ϵ_0 is the free space permittivity, and $\Re\{\cdot\}$ and $\Im\{\cdot\}$ denote the real and imaginary parts of a complex number, respectively. We consider the commonly used insulation of polyvinyl chloride, and use $r_{\mathsf{eff}} = r_{\mathsf{w}} = 4.25$ mm from [23] for our evaluations.

Using the PUL parameters, we compute the characteristic impedance of the line, and TL propagation constant, γ, as [22, Eqs. 6.60, 6.73]

$$Z_c = \sqrt{\frac{R + j2\pi fL}{G + j2\pi fC}}, \tag{6}$$

$$\gamma = \sqrt{(G + j2\pi fC)(R + j2\pi fL)}, \tag{7}$$

where $j = \sqrt{-1}$. We then use γ to obtain [22, Eq. 6.60]

$$I_{\mathsf{net}}(z) = I_{\mathsf{net}}^{+}e^{-\gamma z} + I_{\mathsf{net}}^{-}e^{\gamma z}, \tag{8}$$

where z is the length variable along the line, and I_{net}^{+} and I_{net}^{-} are the forward and backward components of the propagating current I_{net}, respectively. The values of I_{net}^{+} and I_{net}^{-} are contingent on the load conditions that determine the extent of the forward traveling wave that is reflected back, which is captured by the reflection coefficient [22, Ch. 6.2.1].

B. Electric Field Computation

Next, we model the conductor as a concatenation of N Hertzian dipoles, each of whose length $\Delta z \ll \lambda$, where λ is the wavelength of the radiated wave. This setup is also shown in Fig. 3. We then compute the electric field caused due to the nth dipole at a distance d. For computational simplicity, we first represent the generated field in 3-dimensional spherical coordinates $(\hat{\boldsymbol{r}}, \hat{\boldsymbol{\theta}}, \hat{\boldsymbol{\phi}})$ as

$$\begin{aligned}\vec{\boldsymbol{E}}^{(n)}(r_n,\theta_n) &= E_r^{(n)}\ \hat{\boldsymbol{r}} + E_\theta^{(n)}\ \hat{\boldsymbol{\theta}} \\ &= \frac{I_{\mathsf{net}}(-z_n)\Delta z}{2\pi}\eta\left(\frac{1}{r_n} - \frac{j}{kr_n^2}\right)\frac{\exp(-jkr_n)}{r_n}\cos\theta_n\ \hat{\boldsymbol{r}} \\ &+ \frac{I_{\mathsf{net}}(-z_n)\Delta z j\omega\mu}{4\pi}\left(1 + \frac{1}{jkr_n} - \frac{1}{k^2r_n^2}\right)\frac{\exp(-jkr_n)}{r_n}\sin\theta_n\hat{\boldsymbol{\theta}},\end{aligned} \tag{9}$$

where $\eta = 120\pi\ \Omega$ is the free-space impedance, $k = \frac{2\pi}{\lambda}$ is the wave number, and $w = 2\pi f$ is the angular frequency. Further, for the ease adding the field vectors of each of the N dipoles, we convert $\vec{\boldsymbol{E}}^{(n)}$ to Cartesian coordinates $(\hat{\boldsymbol{x}}, \hat{\boldsymbol{y}}, \hat{\boldsymbol{z}})$ as

$$\begin{aligned}\vec{\boldsymbol{E}}^{(n)}(d) &= E_y\ \hat{\boldsymbol{y}} + E_z\ \hat{\boldsymbol{z}} \\ &= \left(\frac{d}{r_n}E_r^{(n)} + \frac{z_n}{r_n}E_\theta^{(n)}\right)\hat{\boldsymbol{y}} + \left(\frac{z_n}{r_n}E_r^{(n)} + \frac{-d}{r_n}E_\theta^{(n)}\right)\hat{\boldsymbol{z}}.\end{aligned} \tag{10}$$

Note that by the orienting the axes in such a way that the dipole stays at the origin and the point-of-interest lies on the $\hat{\boldsymbol{y}} - \hat{\boldsymbol{z}}$ plane, we obtain no component in the $\hat{\boldsymbol{x}}$ direction. We then compute the overall electric field $\vec{\boldsymbol{E}}$ at a perpendicular distance d from the line as the vector sum

$$\vec{\boldsymbol{E}}(d) = \lim_{N\to\infty}\sum_{n=-N}^{N}\vec{\boldsymbol{E}}^{(n)}(d). \tag{11}$$

III. EMI Analysis

In this section, we formulate the limits on the allowed feeding signal based on the maximum electric field regulations. Further, we also examine the effects of the generated $\vec{\boldsymbol{E}}$ on neighboring broadband PLC applications.

A. Electric Field Limits by FCC

Regulatory authorities across the world limit the maximum radiation limits that are tolerable from intentional and unintentional radiation caused in the radio-frequency bands. In our work, we consider the regulations imposed by FCC that is applicable in the North American region in the frequency band of interest between 2 MHz and 30 MHz [19]. Naturally, the same procedure we follow here can also be applied with any specifications.

The Code of Federal Regulations by FCC limits the unintentional radiation by PLC systems to be $\left|\vec{\boldsymbol{E}}_{\mathrm{FCC}}(d = 30\ \mathrm{m})\right| = 30\ \mu\mathrm{V/m}$ [19], [24], [25]. To determine the maximum feeding signal strength using this limit, we first compute the commonly used field coupling factor, $\beta_V = \frac{|\vec{\boldsymbol{E}}|}{|V|}$ [11], by injecting a net current, I_{net}, corresponding to a unit voltage signal, and

determining its associated $\left|\vec{\boldsymbol{E}}(d)\right|$ using (9)−(11). We then set $\left|\vec{\boldsymbol{E}}_{\mathrm{FCC}}(d=30\ \mathrm{m})\right| = 30\ \mu\mathrm{V/m}$ to obtain the voltage and power feeding limits, which we present in Section IV.

B. Impact on Neighboring BB-PLC Applications

Similar to the battery power cables emitting EM radiations as a transmitting antenna, a communication cable located in vicinity of PLC-B is conversely also susceptible to these radiations as a receiving antenna. For a receiving antenna, the incident power density P_{inc} and the maximum received power $P_{\mathsf{R,max}}$ are related by the effective area, i.e., the aperture of the antenna, A, as [26, Eq. 16.3.1]

$$A = \frac{P_{\mathsf{R,max}}}{P_{\mathsf{inc}}}. \tag{12}$$

Further, the aperture A can be expressed with respect to the maximum directivity of the antenna, G_{max}, as [26, Eq. 16.3.5]

$$A = \frac{G_{\mathsf{max}}\lambda^2}{4\pi}, \tag{13}$$

where

$$G_{\mathsf{max}} = \frac{\max\left[U(\theta,\phi)\right]}{\frac{1}{4\pi}\int\limits_{\phi=0}^{\phi=2\pi}\int\limits_{\theta=0}^{\theta=\pi} U(\theta,\phi)\sin\theta \mathrm{d}\theta\mathrm{d}\phi}, \tag{14}$$

with $U(\theta,\phi)$ being the radiant intensity, i.e., the power per unit solid angle.

The incident power density is the magnitude of the Poynting vector of the incident electromagnetic wave. Thus,

$$P_{\mathsf{inc}} = \left|\frac{1}{2}\vec{\boldsymbol{E}}\times\vec{\boldsymbol{H}}\right| = \frac{1}{2}\left|\vec{\boldsymbol{E}}\right|\left|\vec{\boldsymbol{H}}\right| = \frac{1}{2}\frac{\left|\vec{\boldsymbol{E}}\right|^2}{\eta}, \tag{15}$$

where the simplifications arise from the orthogonality of $\vec{\boldsymbol{E}}$ and the magnetic field, $\vec{\boldsymbol{H}}$, and the far-field approximation. From (12), (13) and (15), we get

$$P_{\mathsf{R,max}} = \frac{G_{\mathsf{max}}\lambda^2\left|\vec{\boldsymbol{E}}\right|^2}{8\pi\eta}. \tag{16}$$

Since the power line does not act as an ideal antenna with matched impedance, the practically obtainable received power is $P_{\mathsf{R}} = \kappa P_{\mathsf{R,max}}$, where $\kappa < 1$. This effect can be captured using a reception factor that is defined as

$$\alpha_{\mathsf{rec}} \triangleq 10\log_{10}\left(\frac{\left|\vec{\boldsymbol{E}}\right|^2}{P_{\mathsf{R}}}\right) = 10\log_{10}\left(\frac{8\pi\eta}{\kappa G_{\mathsf{max}}\lambda^2}\right). \tag{17}$$

Note that the term κG_{max} is specific to the considered cable and its location. In order to obtain a realistic value of κG_{max}, we use the measurement results from [27, Ch. 5]. In particular, we set the value of κG_{max} such that the median of α_{rec} over 2 to 20 MHz computed with (17) matches the values presented in [27, Fig. 54][3]. With this procedure, we obtain $\kappa G_{\mathsf{max}} = \frac{1}{20}$.

[3]Although the term κG_{max} could be frequency dependent in practice, we set a fixed value due to the lack of a frequency characterization of α_{rec} in [27, Ch. 5].

Further, with knowledge of the characteristic impedance through (6), we can compute $\left|\vec{\boldsymbol{E}}\right|$ for any transmitted signal with power, P_{T}, using (9)−(11). Thereby, we define the power coupling factor,

$$\beta_P \triangleq 10\log_{10}\left(\frac{P_{\mathsf{R}}}{P_{\mathsf{T}}}\right), \tag{18}$$

which indicates the power of the interference signal that is generated on a neighboring power line as a result of a nearby PLC-B operation with a signal transmitting with a power P_{T}.

Since we use the measured α_{rec} values that are reported for indoor power lines, the results of β_P presented in Section IV are limited to EMI caused on PLC applications. However, we remark that the same procedure is also applicable to characterize EMI on any wired communication network using the associated α_{rec} values.

IV. Numerical Results

In this section, we present the numerical results of nominal radiated emissions, feeding limits, and the extent of interference caused by PLC-B operations on nearby PLC. Throughout this section, we consider a resolution bandwidth of $\Delta f = 9$ kHz to maintain conformity with the measurement apparatus and methods specified in the regulations [19], [28].

A. Increased Radiation

As our first result, we show the increase in electric field caused due to increased separation between the outgoing and the return paths in the PLC-B scenario. First, to determine $\left|\vec{\boldsymbol{E}}(f,d)\right|$ caused by conventional PLC, we feed a signal with a transmit power spectral density of $\widetilde{P}_{\mathsf{TX}} = -50\ \mathrm{dBm/Hz}$, as per the HomePlug AV standard [29]. Accordingly we get the DM current,

$$|I_{\mathsf{DM}}(f)| = \sqrt{\frac{\widetilde{P}_{\mathsf{TX}}\cdot\Delta f}{Z_c}}, \tag{19}$$

for field computation using (8)− (11). To evaluate the worst-case emission, we consider the current close to the feeding point on the cable before the signal has undergone any noticeable attenuation, i.e., $I_{\mathsf{net}}(z,f) = I_{\mathsf{DM}}(f)$, where z is comparatively small. Further, we also assume matched load conditions to let $I^{-}_{\mathsf{net}} = 0$ in (8).

In conventional PLC, where the conductors carrying the outgoing and return currents are in close proximity with each other, the CM current is the primary source of electromagnetic radiation. Thus, we compute a corresponding CM current, $I_{\mathrm{CM}}(f)$, for the DM current of (19) using a longitudinal conversion loss (LCL) factor. Commonly reported LCL values in the literature are between $30-50$ dB [30], [31]. For emulation purposes, we generate Gaussian distributed random CM voltage values (and their corresponding CM currents) across varying frequencies such that the mean and variance of LCL are 40 dB and 5 dB, respectively. We then use $I_{\mathrm{CM}}(f)$ in (9)−(11) to obtain the radiated electric field for conventional PLC, $\left|\vec{\boldsymbol{E}}_{\mathsf{PLC}}(f,d)\right|$. On the other hand, we use the same $\widetilde{P}_{\mathsf{TX}} =$

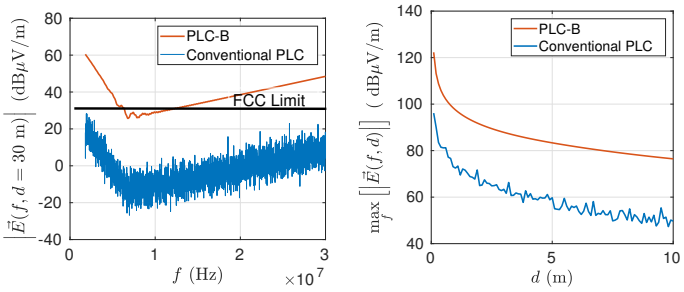

(a) (b)

Fig. 4. Variation of the electric field strength for PLC-B and conventional PLC applications (a) across frequency, and (b) for varying observation distance.

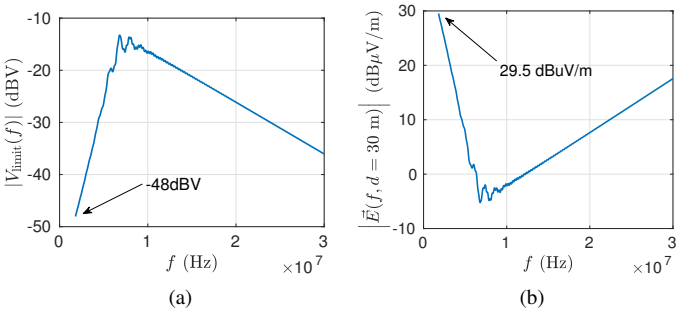

(a) (b)

Fig. 5. (a) Feeding voltage limit across different frequencies that PLC-B devices need to adhere to, in order to conform with the FCC Part 15 emitted radiations regulation, and (b) the obtained electric field strength across all frequencies by injecting a signal of power spectral density -80 dBm/Hz.

-50 dBm/Hz and (19) to get $I_{\mathsf{DM}}(f)$ for use in (8)$-$(11) to obtain $\left|\vec{\boldsymbol{E}}_{\mathsf{PLC-B}}(f,d)\right|$. The field strength results obtained for both applications are shown in Fig. 4(a). The large variation in $\left|\vec{\boldsymbol{E}}_{\mathsf{PLC}}(f, d = 30\ \text{m})\right|$ is a result of the random LCL values that we used in our computations. We can clearly notice that for the same feeding limit of $\widetilde{P}_{\mathsf{TX}} = -50$ dBm/Hz, PLC-B produces about 40 dB of additional radiated emissions, which corresponds to the mean LCL value used. We also notice that while $\left|\vec{\boldsymbol{E}}_{\mathsf{PLC}}(f, d = 30\ \text{m})\right| \leq 30$ dBμV/m, which is the FCC limit for field strength [19], the electric field of PLC-B radiation well exceeds the permitted limits at most frequencies.

Further, in Fig. 4(b), we also plot the variation of the maximum field magnitude across all frequencies, $\max_f \left[\left|\vec{\boldsymbol{E}}_{\mathsf{PLC-B}}(f,d)\right|\right]$ and $\max_f \left[\left|\vec{\boldsymbol{E}}_{\mathsf{PLC}}(f,d)\right|\right]$, between $2-30$ MHz, with the observed distance d. Yet again, we observe that while both values drop with increasing d as anticipated, the radiated emissions from PLC-B is well over the FCC regulations threshold [19].

B. Feeding Limits

To conform to the norms specified in the FCC Part 15 emitted radiations regulations [19], we compute the maximum possible voltage and power spectral density feeding limits, $V_{\mathsf{limit}}(f)$ and $\widetilde{P}_{\mathsf{limit}}$, respectively, using the procedure described in Section III-A. Accordingly, we first compute the field coupling factor as

$$\beta_V(f)\big|_{d=30\ \text{m}} = \left|\vec{\boldsymbol{E}}(f, d = 30\ \text{m})\right|, \tag{20}$$

for a signal of $V(f) = 1$ V on the line. We then determine the feeding limit voltage as

$$|V_{\mathsf{limit}}(f)| = \frac{\left|\vec{\boldsymbol{E}}_{\mathsf{FCC}}(f, d = 30\ \text{m})\right|}{\beta_V(f)\big|_{d=30\ \text{m}}}. \tag{21}$$

In Fig. 5(a), we show the $|V_{\mathsf{limit}}(f)|$ that is permissible on the line to satisfy the radiated emission limits of FCC. We then use $\min_f [V_{\mathsf{limit}}(f)]$ to determine a conservative maximum permissible feeding power spectral density limit as

$$\widetilde{P}_{\mathsf{limit}} = \frac{\left|\min_f [V_{\mathsf{limit}}(f)]\right|^2}{Z_c \Delta f}, \tag{22}$$

in 2 MHz $\leq f \leq$ 30 MHz. Using $\left|\min_f [V_{\mathsf{limit}}(f)]\right| = -48$ dBV shown in Fig. 5(a), we get the $\widetilde{P}_{\mathsf{limit}} = -80$ dBm/Hz. This PSD feeding limit serves as a reference to PLC-B products for compliance with FCC regulations.

Further, in Fig. 5(b), we show the emitted radiation field strength obtained at an observation distance of 30 m from the line, when the injected signal strength is -80 dBm/Hz. We clearly notice that the field strength now lies well within 30 dBμV/m.

C. Interference to Neighboring PLC

As our final result, we show the impact of PLC-B operation on a nearby conventional broadband PLC network, as formulated in Section III-B. We consider different separation distances between the PLC-B and the broadband PLC network, i.e., between a battery cable and a neighboring power line, and plot the power coupling factor, β_P, for different separations in Fig. 6.

We observe that the coupling factor reduces with increase in separation distance as expected. With a nominal separation distance of, say, $d = 10$ m, and an operating power spectral density of $\widetilde{P}_{\mathsf{limit}} = -80$ dBm/Hz as determined in Section IV-B, PLC-B causes a median interference power spectral density of about $-80 - 62 = -142$ dBm/Hz, which is well below most indoor power line noise levels [32], [33]. Fig. 6 also serves as a reference to determine the required physical separation between the battery pack and the indoor electrical wiring installation for any chosen transmission level.

V. Conclusion

We have presented the first analysis of EMC for PLC in energy storage units. By recognizing the unique challenges

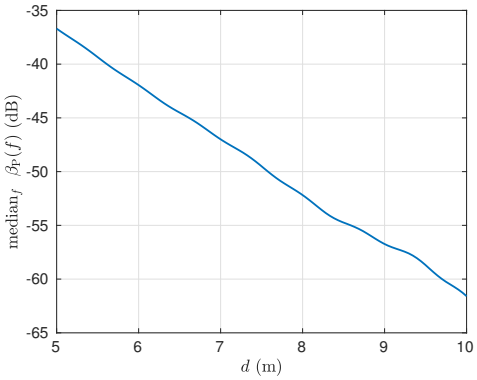

Fig. 6. The median power coupling factor across all frequencies varying with distance of separation.

faced in applying PLC for such scenarios, we derived limits on the signal strength that can be injected on the battery cables to comply with the FCC regulations on radiated emissions. Furthermore, we showed numerical results to determine the feeding PLC-B signal strength and the inter-network separation distance that results in a benign radiated interference with a neighboring broadband PLC network. In conclusion, our work provides a theoretical framework for eventually standardizing PLC operation in energy management systems.

REFERENCES

[1] G. D. Rodriguez, "A utility perspective of the role of energy storage in the smart grid," in *IEEE PES General Meeting*, July 2010, pp. 1–2.

[2] C. A. Hill, M. C. Such, D. Chen, J. Gonzalez, and W. M. Grady, "Battery energy storage for enabling integration of distributed solar power generation," *IEEE Trans. Smart Grid*, vol. 3, no. 2, pp. 850–857, June 2012.

[3] M. C. Such and C. Hill, "Battery energy storage and wind energy integrated into the smart grid," in *IEEE PES Innovative Smart Grid Tech. (ISGT)*, Jan 2012, pp. 1–4.

[4] S. Vazquez, S. M. Lukic, E. Galvan, L. G. Franquelo, and J. M. Carrasco, "Energy storage systems for transport and grid applications," *IEEE Trans. Industrial Electron.*, vol. 57, no. 12, pp. 3881–3895, Dec 2010.

[5] J. Cao and A. Emadi, "A new battery/ultracapacitor hybrid energy storage system for electric, hybrid, and plug-in hybrid electric vehicles," *IEEE Trans. Power Electron.*, vol. 27, no. 1, pp. 122–132, Jan 2012.

[6] H. Rahimi-Eichi, U. Ojha, F. Baronti, and M. Y. Chow, "Battery management system: An overview of its application in the smart grid and electric vehicles," *IEEE Industrial Electron. Mag.*, vol. 7, no. 2, pp. 4–16, June 2013.

[7] D. Lim and A. Anbuky, "A distributed industrial battery management network," *IEEE Trans. Industrial Electron.*, vol. 51, no. 6, pp. 1181–1193, 2004.

[8] A. Scherer, "A smart battery management system for electric vehicles using powerline communication," Master's thesis, Technische Universitat Munchen, Germany, 2013.

[9] J. Jousse, N. Ginot, C. Batard, and E. Lemaire, "Power line communication management of battery energy storage in a small-scale autonomous photovoltaic system," *IEEE Trans. Smart Grid*, vol. 8, no. 5, pp. 2129–2137, 2017.

[10] Y. Maryanka and O. Amrani, "DC powerline communications for management of high voltage battery packs." [Online]. Available: http://yamar.com/articles/Battery-monitoring-system-with-powerline-communication.pdf

[11] H. Hirsch, M. Koch, N. Weling, and A. Zeddam, "Electromagnetic compatibility," in *Power Line Communications: Principles, Standards, and Applications from Multimedia to Smart Grid*, 2nd ed., L. Lampe, A. Tonello, and T. G. Swart, Eds. John Wiley & Sons, 2016, ch. 3, pp. 200–237.

[12] *SIG60 - UART over Powerline for AC/DC Multiplex Network*, Yamar Electronics Ltd, 2010.

[13] I. Ouannes, P. Nickel, and K. Dostert, "Cell-wise monitoring of lithium-ion batteries for automotive traction applications by using power line communication: battery modeling and channel characterization," in *IEEE Int. Symp. Power Line Commun. Appl. (ISPLC)*, 2014, pp. 24–29.

[14] O. Opalko, B. Simon, D. Alonso, and K. Dostert, "Physical layer and multi-carrier analysis for power line communication networks in Li-ion batteries for electric and hybrid vehicles," in *IEEE Veh. Networking Conf. (VNC)*, 2015, pp. 243–250.

[15] N. Recrosio, G. Fine, and M. Helier, "Analysis of radiation characteristics of distribution line carriers with the NEC code," *IEEE Trans. Electromagn. Compat.*, vol. 35, no. 1, pp. 55–68, 1993.

[16] K. Asano, M. Shin, Y. Matsuura, K. Maegawa, S. Yamamoto, and N. Nakayama, "Experimental study of the electromagnetic radiation caused by PLC with high frequency band signals," in *IEEE Int. Symp. Power Line Commun. and its Appl. (ISPLC)*, 2004, pp. 143–148.

[17] E. A. Teixeira and M. V. dos Santos, "PLC-to-LAN interference analysis and electromagnetic shielding," in *IEEE Int. Conf. Emerging Tech. Innovative Business Practices for the Transformation of Societies (EmergiTech)*, 2016, pp. 194–198.

[18] T. Ronkainen, R. Vuohtoniemi, and J.-P. Mäkelä, "Radiated interference of high frequency broadband power line communications," in *IEEE Int. Symp. Electromagn. Compat. (EMC Europe)*, 2014, pp. 555–559.

[19] FCC-Part15, "Radio frequency devices," *FCC, USA*, 2003.

[20] "Power line communication apparatus used in low-voltage installations - Radio disturbance characteristics - Limits and methods of measurement," *EN 50561-1*, pp. 1 –22, 2012.

[21] LINK Personal Communications Programme. (2000) Coupling of EMI to cables: Theory and models. [Online]. Available: http://www.emc.york.ac.uk/reports/linkpcp/appG.pdf

[22] C. R. Paul, *Analysis of multiconductor transmission lines*. John Wiley & Sons, 2008.

[23] Champlain Cable. EXRAD SAE 150 XLE shielded. [Online]. Available: https://www.champcable.com/product/exrad-xle-1000-volt-shielded-cable/

[24] B. Adebisi and B. Honary, "Comparisons of indoor PLC emissions measurement results and regulation standards," in *IEEE Int. Symp. Power Line Commun. and its Appl.*, 2006, pp. 319–324.

[25] P. Pagani, R. Razafferson, A. Zeddam, B. Praho, M. Tlich, J.-Y. Baudais, A. Maiga, O. Isson, G. Mijic, K. Kriznar *et al.*, "Electro magnetic compatibility for power line communications," in *IEEE Int. Sump. Personal Indoor and Mobile Radio Commun. (PIMRC)*, 2010, pp. 2799–2804.

[26] S. J. Orfanidis, *Electromagnetic waves and antennas*. Rutgers University New Brunswick, NJ, 2002.

[27] A. Schwager, "Powerline communications: Significant technologies to become ready for integration," Ph.D. dissertation, Universitat Duisburg-Essen, 2010.

[28] "CISPR 16-1-1 specification for radio disturbance and immunity measuring apparatus and methods; Part 1-1: Radio disturbance and immunity measuring apparatus," *International Electrotechnical Commission*, Nov. 2003.

[29] "Homeplug AV specification, version 1.1," *HomePlug Powerline Alliance*, pp. 1 – 673, May 2007.

[30] A. M. A. Rashid, N. Kuwabara, M. Maki, Y. Akiyama, and H. Yamane, "Evaluation of longitudinal conversion loss (LCL) for indoor AC mains line," in *IEEE Int. Symp. Electromag. Compat.*, vol. 2, 2003, pp. 771–776.

[31] K. See, A. Kamarul, and P. So, "Longitudinal conversion loss of power line network for typical Singapore household," in *IEEE Int. Power Eng. Conf.*, 2005, pp. 1–265.

[32] G. Prasad, H. Ma, M. J. Rahman, F. Aalamifar, and L. Lampe. A cumulative power line noise generator. [Online]. Available: http://www.ece.ubc.ca/~gauthamp/PLCnoise

[33] T. Esmailian, F. Kschischang, and P. Gulak, "In-building power lines as high-speed communication channels: channel characterization and a test channel ensemble," *Int. J. Commun. Syst.*, vol. 16, no. 5, pp. 381–400, 2003.